Review article

Yabin Jin*, Bahram Djafari-Rouhani* and Daniel Torrent*

Gradient index phononic crystals and metamaterials

https://doi.org/10.1515/nanoph-2018-0227
Received December 21, 2018; revised February 8, 2019; accepted February 11, 2019

Abstract: Phononic crystals and acoustic metamaterials are periodic structures whose effective properties can be tailored at will to achieve extreme control on wave propagation. Their refractive index is obtained from the homogenization of the infinite periodic system, but it is possible to locally change the properties of a finite crystal in such a way that it results in an effective gradient of the refractive index. In such case the propagation of waves can be accurately described by means of ray theory, and different refractive devices can be designed in the framework of wave propagation in inhomogeneous media. In this paper we review the different devices that have been studied for the control of both bulk and guided acoustic waves based on graded phononic crystals.

Keywords: gradient index; phononic crystals; metamaterials; lenses; homogenization.

1 Introduction

Phononic crystals and acoustic metamaterials enable to achieve innovative properties for the propagation of mechanical waves (air-borne sound waves, water-borne acoustic waves, water waves, elastic waves, surface acoustic waves and Lamb waves) inapproachable in natural materials. Phononic crystals consist of periodic arrangements of scatterers in a given matrix, and they were firstly proposed in 1993 [1, 2]. The attention that phononic crystals received originally was due to the existence of a phononic Bragg band gap where the propagation of acoustic waves was forbidden. In this regime the wavelength λ of the acoustic field is comparable to the periodicity a of the lattice, $\lambda \approx a$, and to be observable it is also required that the thickness D of the bulk phononic crystals be at least four or five periodicities, $D >> a$. In the subwavelength range, $\lambda >> a$, it is possible to find local resonances in the scatterers, and the designed structures exhibit hybridization band gaps which give rise to novel effects such as negative mass density or negative elastic modulus. In this exotic regime the structure behaves as a special type of materials called "acoustic metamaterials", which were firstly proposed in the seminal work [3] in 2000. Over the past two decades, dramatically increasing efforts have been devoted to the study of acoustic artificial structured materials driven by both fundamental scientific curiosities with properties not found previously and diverse potential applications with novel functionalities [4–16].

While interesting, most of the extraordinary properties of metamaterials are in general single-frequency or narrow-band, since outside the resonant regime metamaterials behave as common composites. However, non-resonant phononic crystals in the low-frequency regime behave as homogeneous non-dispersive materials whose effective parameters can be easily tailored, and in this regime gradient index (GRIN) acoustic materials, or GRIN devices, are easily doable. These devices were firstly proposed for acoustic waves by Torrent et al. in 2007 [17] and for elastic waves by Lin et al. in 2009 [18], and they allow to manipulate acoustic waves to enforce them to follow curved trajectories. They are characterized by a spatial variation of acoustic refractive index, which is designed by locally changing the geometry of units. For instance, the effective index obviously depends on the filling ratio of scatterers, namely, the size of scatterers, which is initially proposed for GRIN control of acoustic waves [17–19]; instead, the variation in the lattice spacing while keeping the size of scatterers

***Corresponding authors: Yabin Jin,** School of Aerospace Engineering and Applied Mechanics, Tongji University, 200092, Shanghai, China, e-mail: 083623jinyabin@tongji.edu.cn. https://orcid.org/0000-0002-6991-8827;
Bahram Djafari-Rouhani, Institut d'Electronique, de Microélectonique et de Nanotechnologie, UMR CNRS 8520, Département de Physique, Université de Lille, 59650 Villeneuve d'Ascq, France, e-mail: bahram.djafari-rouhani@univ-lille.fr;
and **Daniel Torrent,** GROC-UJI, Institut de Noves Tecnologies de la Imatge, Universitat Jaume I, 12071, Castello, Spain, e-mail: dtorrent@uji.es

is also achievable [20, 21]; for triangular shape of scatterers, rotating the angles of the triangular shape can also affect the effective acoustic velocity [22]; for lead-rubber pillared metamaterial plate, by changing the height of lead layer in pillars, the effective mass density is tuned, resulting in a change in effective phase velocity following a given law [23]; for phononic crystal plates, the effective velocity of antisymmetric Lamb wave is directly related with the thickness of plates, which can also further affect the effective velocity of symmetric mode [24–26]; and gradient effective index can also be achieved from coiling-space structures [27–30]. In addition to the geometric parameters, the effective refractive index can also be tuned in relation to the elastic properties of the scatterers, for instance, the choice of materials [18, 31], or to an external stimulus such as electric field [32] or temperature [33].

The attained effective refractive index of the GRIN device can be smaller or larger than that of the background medium, which corresponds to phase advance [20] or delay approaches in wave propagation. Nevertheless, the phase delay approach is mostly employed as higher refractive index enables to design more advanced functionalities and reduce the entire width of the devices. Comparing to the wavelength, the thinner the device, the larger will be the highest required index. If the width of the whole device is downscaled to the subwavelength regime, the GRIN device becomes a metasurface [34, 35]. However, to find a high enough effective refractive index to design GRIN metasurfaces is a big challenge that needs new technologies in material science. Recently, it has been reported that soft porous materials [36, 37] with soft-matter techniques can achieve a relative refractive index higher than 20 [38], resulting in soft GRIN metasurface [39]. GRIN devices can also be designed with negative index of refraction at frequencies lying in the first negative slope of the acoustic band structure [21]. However, these devices would have a narrow band, and it may limit potential applications.

GRIN phononic crystals and metamaterials can be applied to various types of waves in a long frequency limit, such as surface water waves [40, 41] for a few hertz, air-borne sound waves [19, 42–51] for 10^3–10^5 Hz, water-borne acoustic waves [20, 31, 52–54] for 10^4–10^6 Hz, Rayleigh waves [55–59] for 10–10^8 Hz and Lamb waves [23–25, 32, 60–72] for 10^3–10^8 Hz, among others, with functionalities like focusing [18, 19], waveguiding [70, 73], mirage [74], beam splitting or deflection [41, 62, 63], cloaking [55, 64] or energy harvesting [71, 72, 75]. It is in the domain of elastic waves in plates where the most interesting applications at the nanoscale are found, since from the technological point of view low-dimensional materials are more interesting than bulk materials. The excellent compatibility of phononic crystals and metamaterials with the nanoelectromechanical systems has been proven for applications in wireless telecommunications, sensing or thermal control, among others [76–81]. However, the propagation of elastic waves in plates is in general composed of three polarizations, which travel at different speeds and for which refractive devices designed for one of these polarizations will not work for the other two. Recently, the designs of GRIN devices based on phononic crystal plates have demonstrated that the simultaneous control of all fundamental modes propagating in thin elastic plates in a broadband frequency region is possible [25, 26, 63].

The objective of this review is to provide a comprehensive picture of the evolution of the domain of GRIN devices for mechanical waves, to demonstrate the wide variety of applications at the nanoscale that these devices offer and to present the challenges to be accomplished to further develop this field. The paper is organized as follows: after this introduction, we will review the fundamental ideas of the homogenization of sonic and phononic crystals in Section 2 and of phononic crystal plates in Section 3, which offers efficient tools to obtain the effective elastic properties and, consequently, their effective refractive index. Then we will review GRIN devices for bulk acoustic and elastic waves in Section 4 and for flexural waves in Section 5; the advanced full control of polarizations in elastic plates with multimodal GRIN devices will be reviewed in Section 6. The last section will present some conclusions and future challenges.

2 Homogenization of sonic and phononic crystals

Graded materials with specific variations of the refractive index are obviously not found in nature, and they have to be artificially engineered. The inclusion of scatterers in a given matrix is an excellent way for the realization of artificially graded materials, since the average behavior of the scatterers is to modify the effective velocity of acoustic waves in the matrix, and this effective velocity can be tuned by means of the size of the inclusions. When these inclusions are arranged in a regular array we call the composite a sonic (fluid matrix) or phononic (solid matrix) crystal, and the computation of the effective sound velocity is made by a set of mathematical tools called

homogenization theories. Roughly speaking, the homogenization region is the range of frequencies at which the propagating field cannot distinguish the individual scatterers of the composite and perceives the structure as a uniform material with some effective parameters (stiffness constant, mass density, viscosity, etc. are the parameters to be computed by means of the most adequate homogenization method).

Homogenization is an old problem, and a great bibliography is available in this realm (see for instance [82]). Our aim here is not to review all these methods but to present some examples of these methods applied to the specific case of sonic and phononic crystals.

2.1 Homogenization of sonic crystals by multiple scattering theory

As mentioned before, a sonic crystal consists of a periodic distribution of solid or fluid inclusions embedded in a fluid matrix. When the operating wavelength is larger than the typical distance between inclusions (lattice constant) the field cannot distinguish individual scatterers and perceives the structure as a homogeneous material with some effective parameters (mass density, compressibility, speed of sound etc). There exists a vast literature about homogenization of periodic and random materials [82], but it has been shown that multiple scattering theory is a versatile method in the case of sonic crystals. For instance, for the simple case of a two-dimensional arrangement of fluid inclusions (parameters labeled with "a") in a fluid background (parameters labeled "b"), the effective bulk modulus B_{eff} and mass density ρ_{eff} are given by

$$\frac{1}{B_{\text{eff}}}=\frac{f}{B_a}+\frac{1-f}{B_b},\ \frac{\rho_{\text{eff}}}{\rho_b}=\frac{\rho_a(\Delta+f)+\rho_b(\Delta-f)}{\rho_a(\Delta-f)+\rho_b(\Delta+f)} \tag{1}$$

where f is the filling fraction of the crystal (area of the inclusions divided by the area of the unit cell) and Δ represents a modification of the filling fraction due to the multiple scattering processes [83, 84].

For airborne propagation any solid material will have a much higher density than that of air, and the extreme impedance mismatch blocks the penetration of the acoustic wave into the solid inclusions. Therefore, those solids can be assumed to be "rigid" inclusions, and their mass density and compressibility can be set as infinite. In this case, if the filling fraction is small and the multiple scattering interactions can be neglected (Δ can be regarded as 1) the effective mass density and velocity can be simplified as [83]

$$\rho_{\text{eff}}=\frac{\rho_{\text{air}}(1+f)}{1-f},\ c_{\text{eff}}=c_{\text{air}}/\sqrt{1+f} \tag{2}$$

and we recover the effective mass density and effective sound velocity derived by Barryman [85] and the heuristic model [86], respectively.

As an example of application, a circular cluster of 151 wooden cylinders arranged in a hexagonal lattice embedded in air was homogenized by multiple scattering, and the resulting effective parameters as a function of the filling fraction are shown in the left panel of Figure 1.

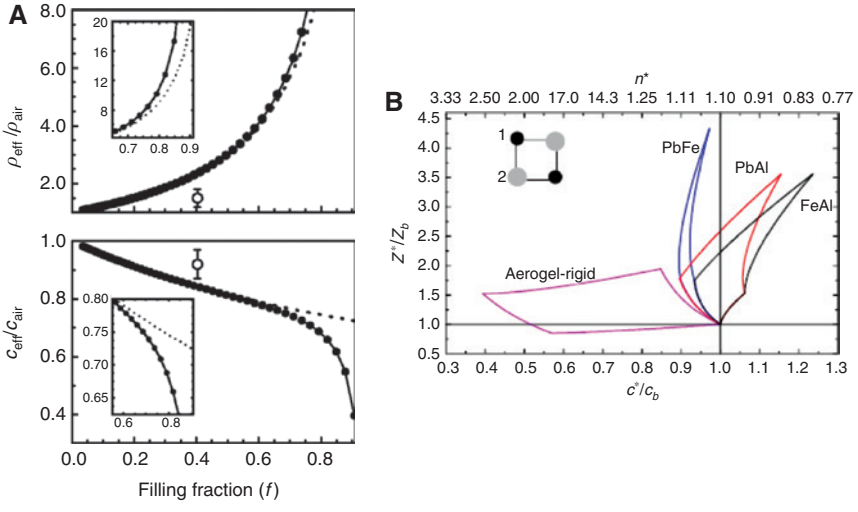

Figure 1: Effective elastic parameters of sonic crystals.
(A) Effective mass density and effective sound velocity for a circular cluster consists of 151 rigid cylinders embedded in air. The black dots stand for the results from the multiple scattering simulations in Eq. (1), and the dashed lines are values obtained from Eq. (2) [83];
(B) Impedance-velocity diagram of sonic crystals consist of square lattice of solids 1 and 2 cylinders in air. Insert shows the unit cell [87].

We can clearly observe, especially from the insets, that the simplified approach by Eq. (2) for effective mass density is valid when the filling fraction is no larger than 0.7; meanwhile, the maximum limit of filling fraction is 0.6 for effective sound velocity. Experiments verified the homogenization method, and it was shown that for wavelengths larger than 4 times the lattice constant, the cluster could be considered as a homogeneous cylinder with fluid-like properties [83].

The theory can be generalized to more cylinders per unit cell. If we consider two types of cylinders, with materials labeled as 1 and 2, embedded in a square lattice, their fluid-like parameters being (ρ_{a1}, B_{a1}) and (ρ_{a2}, B_{a2}) and the filling fractions being f_1 and f_2, respectively, the effective parameters can be obtained as

$$\frac{1}{B_{\text{eff}}}=\frac{1-f}{B_b}+\frac{f_1}{B_{a1}}+\frac{f_2}{B_{a2}},\ \rho_{\text{eff}}=\frac{1+f_1\eta_1+f_2\eta_2}{1-f_1\eta_1-f_2\eta_2}\rho_b,\ c_{\text{eff}}=\sqrt{\frac{B_{\text{eff}}}{\rho_{\text{eff}}}} \tag{3}$$

where $f=f_1+f_2$, $\eta_i=(\rho_i-\rho_b)/(\rho_i+\rho_b)$.

The right panel of Figure 1 shows a "phase diagram" of the effective impedance and effective sound velocity for several selected pairs of materials under the low filling fraction condition (neglecting multiple scattering interactions), for different pair of materials and backgrounds (Pb-Fe, Pb-Al and Fe-Al in water and aerogel-rigid cylinders in air). Any point on each curve is calculated sweeping over the total filling fraction. The overlapped corner point (1, 1) in this diagram corresponds to the case of $f_1=0$ and $f_2=0$. Notice that the effective impedance matches that of the background when the sonic crystal is made of aerogel and rigid cylinders embedded in air, making the sonic crystal transparent to air possessing a different refractive index. This interesting property was used in ref [17] to design a completely transparent GRIN lens.

Multiple scattering allows the homogenization of finite clusters; therefore, it is a versatile method to study the behavior of the effective parameters when disorder is introduced in the lattice [84] or even the effect of the cluster's size, as it was done in Ref. [88], where it was found that small clusters with specific number of scatterers presented the same effective parameters as that of the infinite medium.

2.2 Homogenization of periodic phononic crystals

Metamaterials for acoustic or elastic waves have been mainly studied by means of sonic or phononic crystals. As said before, in the low-frequency limit, an anisotropic phononic crystal behaves as a homogeneous material with some effective parameters. The plane wave expansion (PWE) method is an alternative method to multiple scattering for the homogenization of periodic composites. This approach was firstly proposed by Krokhin [89] for sonic crystals and generalized for non-local phononic crystals in [90]. The equation of motion of a homogeneous elastic material assuming harmonic time dependence is given by [91]

$$\rho\omega^2 u_i=k^2 n_{iI}C_{IJ}n_{Jj}u_j \tag{4}$$

where ρ is the mass density, ω is the angular frequency, u_i is the displacement, k is the wavenumber, $\boldsymbol{n}$ is a unit vector, $\boldsymbol{C}$ is the stiffness tensor, and we use Voigt notation for the sub-indexes.

In a phononic crystal the mass density and stiffness tensors are periodic functions of the spatial coordinates, and an inhomogeneous version of the above equation has to be used. The PWE method is applied and then we arrive to an eigenvalue equation [92]

$$\omega^2\rho_{\boldsymbol{G}-\boldsymbol{G}'}(u_{\boldsymbol{G}'})_i=(\boldsymbol{k}+\boldsymbol{G})_{iI}C_{IJ}^{\boldsymbol{G}-\boldsymbol{G}'}(\boldsymbol{k}+\boldsymbol{G}')_{Jj}(u_{\boldsymbol{G}'})_j \tag{5}$$

where $\rho_{\boldsymbol{G}}$, $C_{IJ}^{\boldsymbol{G}}$ and $(u_{\boldsymbol{G}'})_i$ are the Fourier components of the mass density, stiffness tensor and the displacement field, respectively. The summation over repeated indexes has been assumed. The above equation can be manipulated to solve for the average field ($\boldsymbol{G}=0$ component), and this average field can be used to describe the effective behavior of the crystal. Then, after some complex mathematical manipulation we arrive to an expression for the dispersion relation of the average field, which consists in calculating the roots of the determinant of the matrix Γ as

$$\Gamma_{ij}=\omega^2\rho_{ij}^*-k^2 n_{iI}C_{IJ}^*n_{Jj}-\omega k(n_{iI}S_{Ij}+S_{ij}^{\dagger}n_{Jj}) \tag{6}$$

where the effective mass density ρ_{ij}^*, the effective stiffness C_{IJ}^* and the coupling tensor S_{Ij} are [92]

$$\rho_{ij}^*(\omega,k)=\overline{\rho}\delta_{ij}+\omega^2\rho_{-\boldsymbol{G}'}\chi_{ij}^{\boldsymbol{G}'\boldsymbol{G}}(\omega,k)\rho_{\boldsymbol{G}} \tag{7a}$$

$$C_{IJ}^*(\omega,k)=\overline{C}_{IJ}-C_{IL}^{-\boldsymbol{G}}(k+\boldsymbol{G}')_{Ll}\chi_{\text{lm}}^{\boldsymbol{G}'\boldsymbol{G}}(\omega,k)(k+\boldsymbol{G})_{mM}C_{MJ}^{\boldsymbol{G}} \tag{7b}$$

$$S_{Ij}(\omega,k)=\omega C_{IL}^{-\boldsymbol{G}}(k+\boldsymbol{G}')_{Ll}\chi_{\text{lj}}^{\boldsymbol{G}'\boldsymbol{G}}(\omega,k)\rho_{\boldsymbol{G}} \tag{7c}$$

The above formulas offer a way to describe resonant ($\chi_{\boldsymbol{G}\boldsymbol{G}'}$) and nonlocal ($k$) phononic crystals. In the

low-frequency ($\omega \to 0$) and local ($k \to 0$) limit, from Eq. (7), the coupling tensor $S_{Ij}=0$; the mass density is a scalar as the volume average value, the effective stiffness tensor is simplified as

$$\rho^{\star}_{ij} = \overline{\rho}\delta_{ij},\ C^{\star}_{IJ} = \overline{C}_{IJ} - C^{-\boldsymbol{G}'}_{IL}\boldsymbol{G}'_{Ll}(M^{-1}_{\boldsymbol{G}'\boldsymbol{G}})^{\boldsymbol{G}'\boldsymbol{G}}_{\mathrm{lm}}\boldsymbol{G}_{mM}C^{\boldsymbol{G}}_{MJ} \tag{8}$$

The expressions derived there can also be applied in the low-frequency limit to obtain the following effective parameters

$$\rho_{\mathrm{eff}} = (1-f)\rho_b + f\rho_a \tag{10a}$$

$$D_{\mathrm{eff}}(1+\nu_{\mathrm{eff}}) = \frac{(1+\nu_b)[D_b(1-\nu_b)+D_a(1+\nu_a)] - f(1-\nu_b)[D_b(1+\nu_b)-D_a(1+\nu_a)]}{D_b(1-\nu_b)+D_a(1+\nu_a) - f[D_b(1+\nu_b)-D_a(1+\nu_a)]}D_b \tag{10b}$$

$$D_{\mathrm{eff}}(1-\nu_{\mathrm{eff}}) = \frac{(1-\nu_b)[D_b(3+\nu_b)+D_a(1-\nu_a)] - f(3+\nu_b)[D_b(1-\nu_b)-D_a(1-\nu_a)]}{D_b(3+\nu_b)+D_a(1-\nu_a) - f[D_b(1-\nu_b)-D_a(1-\nu_a)]}D_b \tag{10c}$$

where $(M_{\boldsymbol{G}'\boldsymbol{G}})_{ij} = G_{iI}C^{\boldsymbol{G}-\boldsymbol{G}'}_{IJ}G'_{Jj}$. The information about the details of the phononic crystal structures is included in the stiffness tensor whose symmetry relates with the background matrix, inclusion, and lattice symmetry.

Periodic homogenization is therefore a versatile calculation method of the effective parameters, where once we know the shape of the scatterer or scatterers in the unit cell we can Fourier-transform their spatial distribution and obtain the effective parameters. The major drawback of this method is that it is not suitable for high contrast of inclusions or fluid-elastic composites, since in this case convergence is poor. Also, due to periodicity, order-disorder effects are not easy to study. It is therefore a complementary technique to the multiple scattering method presented in the previous section.

3 Homogenization of phononic crystal plates

In a homogeneous thin elastic plate, the propagation of flexural waves (antisymmetric Lamb mode wave) can be approximately described by the bi-Helmholtz equation (assuming time harmonic dependence of the field)

$$(D_b\nabla^4 - \rho_b h_b\omega^2)W(x,y) = 0 \tag{9}$$

where ρ_b, h_b and $D_b = E_b h_b^3/12(1-\nu_b^2)$ are the mass density, the thickness and the rigidity of the plate, respectively, E_b being the Young's modulus and ν_b the Poisson's ratio. W is the out of plane displacement field. Multiple scattering can also be applied for the homogenization of distribution of scatterers in elastic plates, and frequency-dependent effective parameters were obtained in [61]. where the subscript "a" ("b") means the parameters for inclusions (background). The effective phase velocity can be obtained by the ratio of the wavenumber between the effective medium and the background, giving

$$\frac{c_{\mathrm{eff}}}{c_b} = \frac{k_b}{k_{\mathrm{eff}}} = \frac{(D_{\mathrm{eff}}/\rho_{\mathrm{eff}})^{1/4}}{(D_b/\rho_b)^{1/4}} \tag{11}$$

As an example, let us consider circular inclusions in a thin aluminum plate ($h_b = 0.1a$) and let the inclusion's material be chosen as a hole (empty inclusion), lead and rubber, whose parameters can be found in Ref. [61]. The effective parameters as given by Eqs. (10) and (11) as a function of the filling fraction are plotted in the left panel of Figure 2. The effective mass density is the volume average approach as for bulk waves. We see that the effective rigidity and the Poisson's ratio for the case of rubber behaves like that of a hole, since the ratio of the Young's modulus between the rubber and the aluminum is very low. For the effective phase velocity, the difference between the rubber and the hole is more evident. In the right panel of Figure 2 is shown the dispersion curves from finite element methods (red dots) and the effective parameters in Eq. (10) (blue lines) for a triangular lattice of hole/lead inclusions in a thin aluminum plate with the radius of inclusion being $0.3a$. We can clearly observe that the agreement between the numerical simulation and the effective theory is quite good for the antisymmetric (A_0) and symmetric (S_0) Lamb modes. This is remarkable since we have developed the theory for the antisymmetric mode only; however, there is a connection between the speed of these two modes [26] if a wave propagates from plate h_1 to plate h_2, $n_A^2 = n_S\frac{h_1}{h_2}$, which allow us to relate both, even if the propagation of the S mode has not been included in the theory.

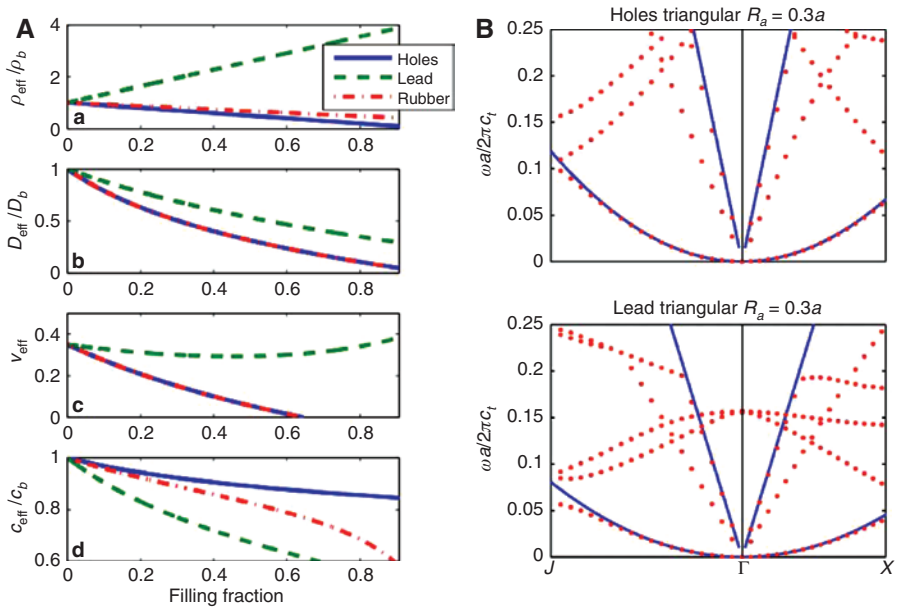

Figure 2: Effective elastic parameters of phononic crystal plates.
(A) The effective mass density (a), rigidity (b), Poisson's ratio (c) and phase velocity (d) with respect to the filling fraction for different cylinder inclusions in an aluminum plate [61]; (B) Dispersion relations for a phononic crystal plate made of a triangular lattice of circular holes and lead inclusions with a radius of 0.3a. The red dots show the band structures obtained by the finite element method, while the blue lines show the dispersion curves calculated with homogenized parameters from Eq. (10) [26].

Actually, there are three fundamental plate modes as it is seen in the right panel of Figure 2, with the third one named shear-horizontal mode (SH_0), which needs an additional effective stiffness component c_{66}^{eff} to compute its dispersion relation. The theory developed for flexural waves allows the calculation of the velocity of the S_0 mode only due to the special relationship between the velocities of A_0 and S_0 modes; however, a similar relationship is not found, or at least obvious, for the SH mode. However, the homogenization theory for bulk phononic crystals presented in Section 2.2 offers the full components of the effective stiffness matrix, and it can be used to compute the effective velocity of shear waves in a phononic crystal plate. This connection is not obvious in principle; however, it can be explained by a two-step homogenization procedure.

Figure 3, upper left panel, shows a two-dimensional phononic crystal made of cylinders embedded in a bulk matrix. The phononic crystal plate at the upper right panel can be regarded as a finite "slice" taken from the bulk phononic crystal. In the low-frequency limit, the phononic crystal behaves as a homogeneous material with effective parameters and tetragonal anisotropy (square lattice) or transversal isotropy (triangular lattice), and this symmetry is maintained for the phononic crystal plate, as illustrated from the upper panel to the lower panel in Figure 3A. Thus, the effective phononic crystal plate can also be considered as a finite "slice" of the effective homogeneous material with the same symmetry. Such homogenization procedure has a non-trivial implication in accordance with symmetry.

As an example, a phononic crystal plate with the unit cell shown in Figure 3B is considered for three different thicknesses, consisting of hole-gold shell unit cell in triangular lattice. The inner radius is 0.2a, while the outer radius is 0.4a. The dispersions obtained from homogenization method with effective parameters in Eq. (8) are compared to those from finite element methods, as displayed in Figure 3B. In the low-frequency limit, these effective phononic crystal plates behave like transversely isotropic plate. It is clear that the agreements between the finite element method and homogenization method are excellent for S_0 and SH_0 modes for all cases of thickness before the mode branches deviate, as their dispersions do not depend on the plate's thickness. However, the dispersion of A_0 mode relates with the plate's thickness. For thinner plates, the dispersion of fundamental A_0 mode keeps the parabolic shape throughout the Γ-J direction of the first irreducible Brillouin zone, so that there is an excellent agreement in the whole range of Γ-J for plate's thickness as 0.1a. For thicker thickness such as 0.5a and a, the agreement for A_0 mode goes well before the A_0 mode branch deviates.

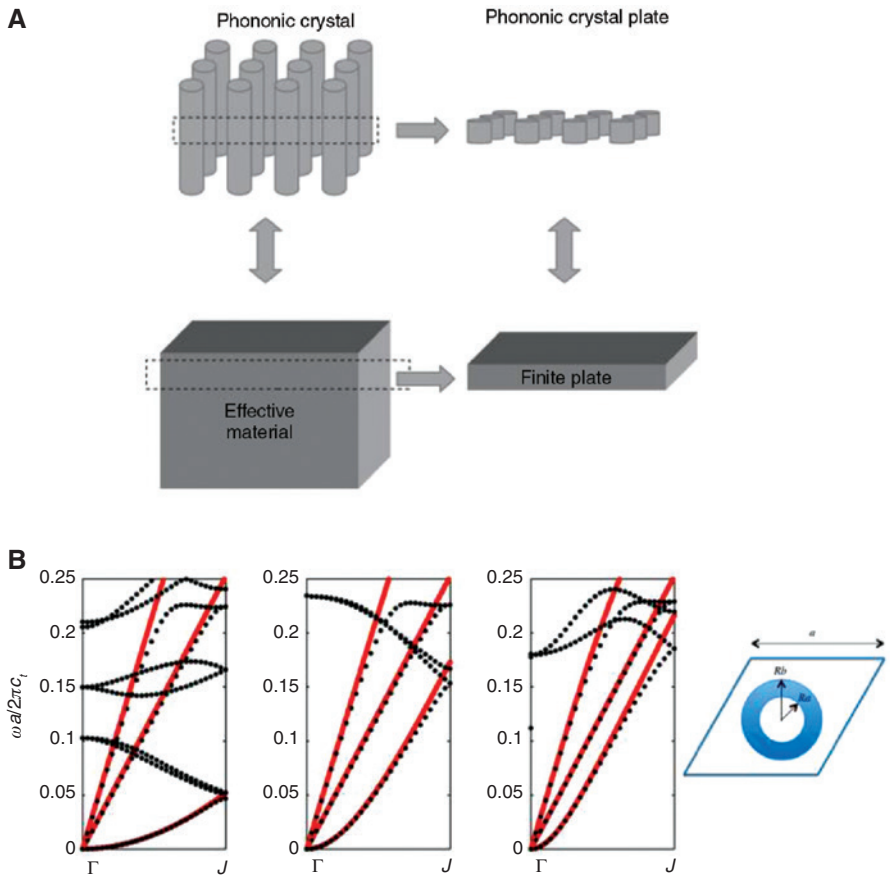

Figure 3: Homogenization of phononic crystal plates for all three fundamental Lamb modes.
(A) Illustration of the homogenization relationship between phononic crystal and phononic crystal plate [26]. (B) Dispersion comparison of a phononic crystal plate between the finite element method (black dots) and the homogenization theory with effective parameters from Eq. (8) (red lines) for the plate thickness as 0.1*a* (left), 0.5*a* (middle) and *a* (right). The phononic crystal plate consists of a triangular lattice of hole-gold shell unit cell whose inner radius is 0.2*a* and outer radius is 0.4*a* [25].

As a conclusion, the homogenization procedure for phononic crystal plates illustrated in Figure 3A works well for low-frequency limit and thin plates.

4 GRIN devices for bulk acoustic and elastic waves

This section is devoted to the review of GRIN devices for waves in bulk materials; therefore, no interfaces are assumed and surface or guided waves are excluded in this section (they will be considered in the next one). In principle we could divide the devices into two types, depending on the nature of the matrix which can be fluid or solid. This division makes sense since in the former shear waves does not exist in the background and the field is described entirely by a scalar pressure field, while in the latter shear waves with different propagation velocities have to be as well considered. However, for the fluid matrix an additional division can be made, since the physics involved in the scattering process is different if the background is air or water. While in air almost all solid materials are acoustically rigid due to the impedance mismatch between air and any solid, in underwater acoustics this impedance mismatch is of the same order, so that we have to consider the elastic nature of the inclusions. For this reason, we divide this section into three subsections, corresponding to the study and design of GRIN devices for air, water and solid backgrounds.

4.1 GRIN devices for bulk acoustic waves in air

In this section, we will discuss the flat GRIN lens for focusing whose surface is flat instead of being curved as in traditional lenses.

The index profile of GRIN flat lenses keeps constant along the propagating x axis while it changes along the vertical y axis as [18]

$$n(y) = n_0 \mathrm{sech}(\alpha y),\ \alpha = \frac{1}{h}\cosh^{-1}\left(\frac{n_0}{n_h}\right) \tag{12}$$

where h is the half-height in y axis of the lens, n_0 is the refractive index at $y=0$, and n_h is the index at the upper or lower edges $y=\pm h$. Such index profile is designed with the aim of presenting low aberrations [18]. The position of focal point x_f at the right side of the lens can be derived from the differential equation satisfied by the energy rays [19].

As shown in Figure 4A, a GRIN lens was fabricated with nine columns of metal rods whose radii are varied locally by an inverse design as follows: first make a sweep of the filling fraction for sonic crystals made of rigid cylinders to plot the diagram of effective index and the filling fraction; then calculate the required index at a given position along the y axis of the GRIN lens; next, choose the corresponding filling fraction of the rigid cylinder from the diagram in the first step in accordance with the required index in the second step; finally, calculate the required radius from the selected filling fraction in the third step. Figure 4B shows the pressure distribution fields after the GRIN sonic crystal at a frequency corresponding to a wavelength of about 3.8a numerically (upper panel) and experimentally (lower panel). Similar focal spots and side lobes are evidently seen. To quantitatively characterize the focusing effect, the pressure along the x and y axes are also plotted in Figure 4C, showing very good agreements. In this approach with rigid cylinders in GRIN sonic lenses, the effective impedance of the lens is not matched with the background, so that the maximum pressure at the focal spot is limited. As indicated in Figure 1B in Section 2.1, the mixed lattice of aerogel and rigid cylinders can also tailor the effective index while keeping the effective impedance matched with the background, so that zero reflectance can be achieved to make the lens transparent. The first GRIN sonic Wood lens proposed in Ref. [87] has a higher pressure focalization at the focal spot.

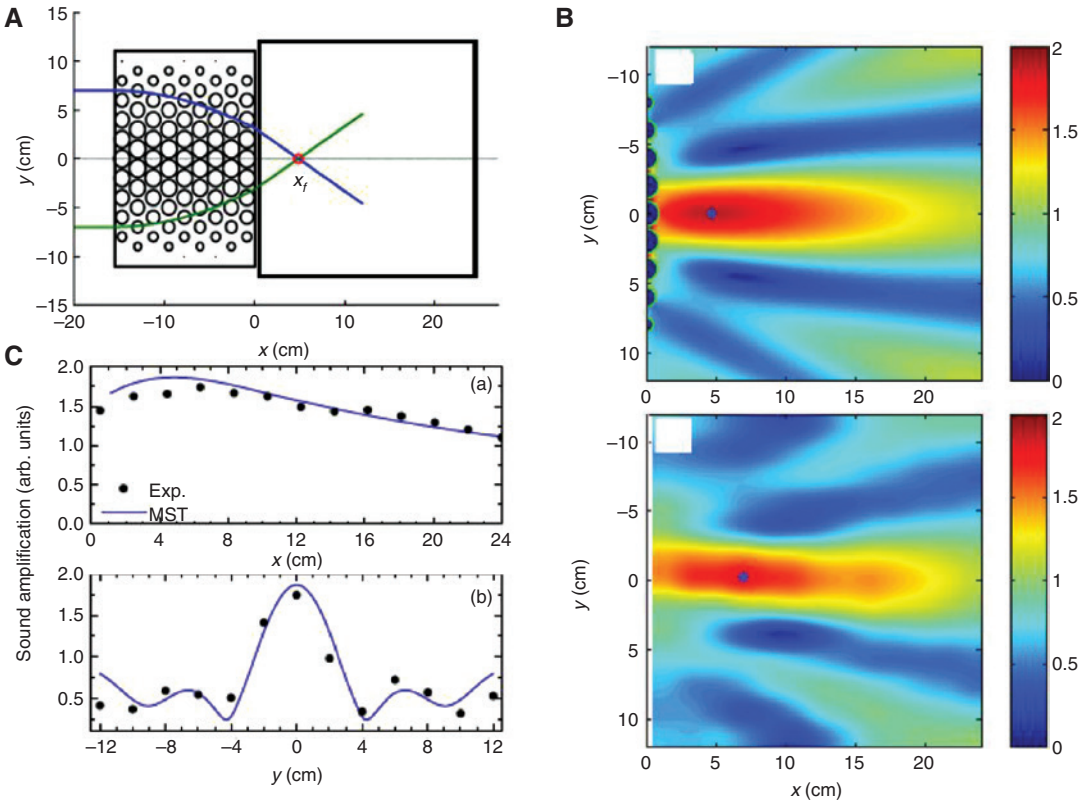

Figure 4: Sonic GRIN flat lens.
(A) Schematic view of a GRIN lens with the ray trajectory. For the impinging plane sound wave, the rays will bend and focus at x_f position at the right side of the lens. (B) Normalized sound amplitude at 4.5 kHz mapped at the right side of the GRIN lens from the multiple scattering method (upper panel) and the experiment (lower panel). (C) Normalized sound amplitude along the x and y axes crossing the focusing point. Blue lines stand for simulation, and black dots stand for experiment [19].

4.2 GRIN devices for bulk acoustic waves in water

Different from the impedance mismatch between the air and solid scatters, the mass density and acoustic velocity are in the same order for most scatterers and water, so that the scatters cannot be regarded as rigid anymore. From Eq. (1) in Section 2.1, one can also calculate the effective parameters of phononic crystals in water.

For the same type of GRIN flat lens as in the last section, similar phononic crystals made of radius-varied steel cylinders are proposed in water [93]. In the upper left panel in Figure 5, the profile of radius is calculated to meet the required index profile like Eq. (12), the maximum index being at the center and minimum at the edges in vertical axis. A plane wave with center frequency at 20 kHz is excited, corresponding to wavelength as 4 times lattice constant around the cutoff frequency in the low-frequency limit. A clear focusing spot is observed from the experimental pressure intensity field. From the multiple scattering theory(MST) simulation, a similar position focal spot is also obtained as shown the dot "+" in subpart (c) of upper right panel of Figure 5. It is worthy to note that this GRIN lens also supports the source off the central axis, which was demonstrated numerically and experimentally [93].

Equation (12) gives a picture of special index profile for focusing with low aberration, while it does not define that the maximum index at the center n_0 should be larger than that of the background n_b; in another word, Eq. (12) can also be achieved by phase advance approach. In the lower panel of Figure 5, phononic crystals made of air-filled aluminum tubes are arranged in water with anisotropic

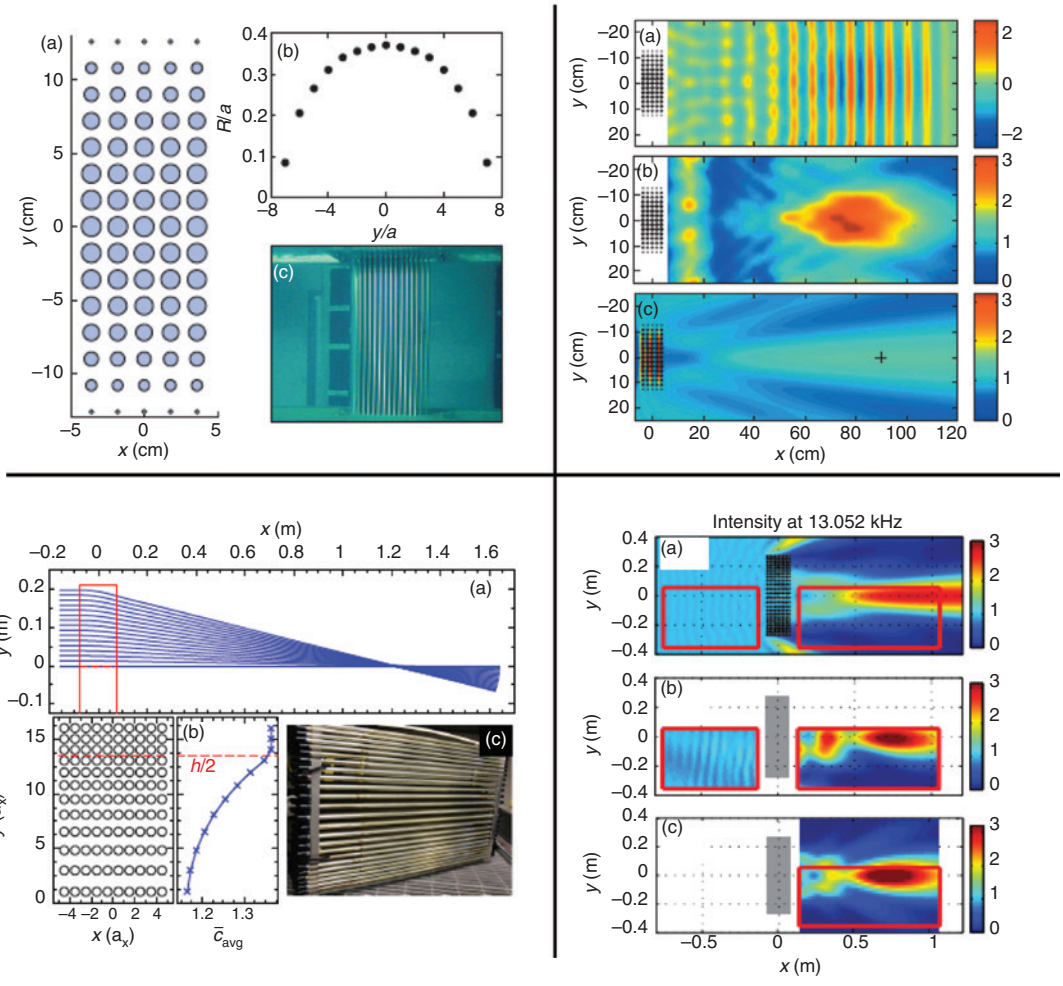

Figure 5: GRIN flat lens with phase delay and advance approaches.
Upper left panel: Schematic view of GRIN flat lens with radius-varied steel cylinders embedded in water. Upper right panel: Normalized pressure amplitude from the source (a), measured normalized pressure intensity after the GRIN lens (b) and the same pressure intensity map using MST (c) [93]. Lower left panel: Schematic view of GRIN flat lens made of the same hollow air-filled aluminum tubes with anisotropic lattice spacing. Lower right panel: Sound pressure intensity at 13.05 kHz from 2D MST (a), experiment (b) and 3D Rayleigh-Sommerfeld approximation (c) [20].

lattice spacing. The thickness of the aluminum shell is 1/10 of the radius that is designed to have impedance matching with respect to water [94], a higher velocity but lower mass density acting as metafluids. The required filling fraction profile to meet the index distribution is implemented by using anisotropic lattice spacing [95]. From the lower left panel of Figure 5, the lattice space in vertical axis is large at the center while it reaches the minimum at the upper and lower edges. The minimum velocity at the center is still larger than that of the background water, resulting in a phase advance GRIN lens. A good comparison is found in the lower right panel of Figure 5 among the experimental measurement and two predicted numerical simulations. It is worth mentioning that such GRIN flat lens is broadband, which can be implemented in water from experimental point of view as the short pulse from the transducer in water is normally broadband.

4.3 GRIN devices for bulk elastic waves

The effective parameters for bulk elastic wave in 2D phononic crystals can be found in Eq. (8) in Section 2.2. Here, another approach based on the analysis of the lowest band among the dispersion curves is introduced. Let us consider a phononic crystal made of square lattice solid inclusions embedded in an elastic matrix. For small anisotropic ratios, the effective index for a bulk elastic wave can be obtained as [18]

$$n_{\text{eff}} = \frac{n_{\Gamma X} + n_{\Gamma M}}{2},\ n_{\Gamma X} = \frac{c_b}{c_{\Gamma X}} = \frac{c_b}{d\omega/dk_{\Gamma X}},\ n_{\Gamma M} = \frac{c_b}{c_{\Gamma M}} = \frac{c_b}{d\omega/dk_{\Gamma M}} \tag{13}$$

where c_b is the acoustic velocity in the background matrix, c is the group velocity of the bulk elastic wave mode, and ΓX and ΓM are two orientations in the first Brillouin zone. For an epoxy matrix phononic crystal, the diagram of the first band of shear-vertical (SV) mode is plotted in two ways: (i) steel inclusions with different filling fractions (different radii) as shown in the left panel of Figure 6A; and (ii) fixed filling fraction but with different material inclusions as shown in the right panel of Figure 6A. The elastic parameters for different solid materials can be found in Ref. [18]. Both approaches can change the slope of the first SV mode leading to a variation of effective index by Eq. (13).

From the dispersion curve variations, for a given band the effective index will change locally along the reduced

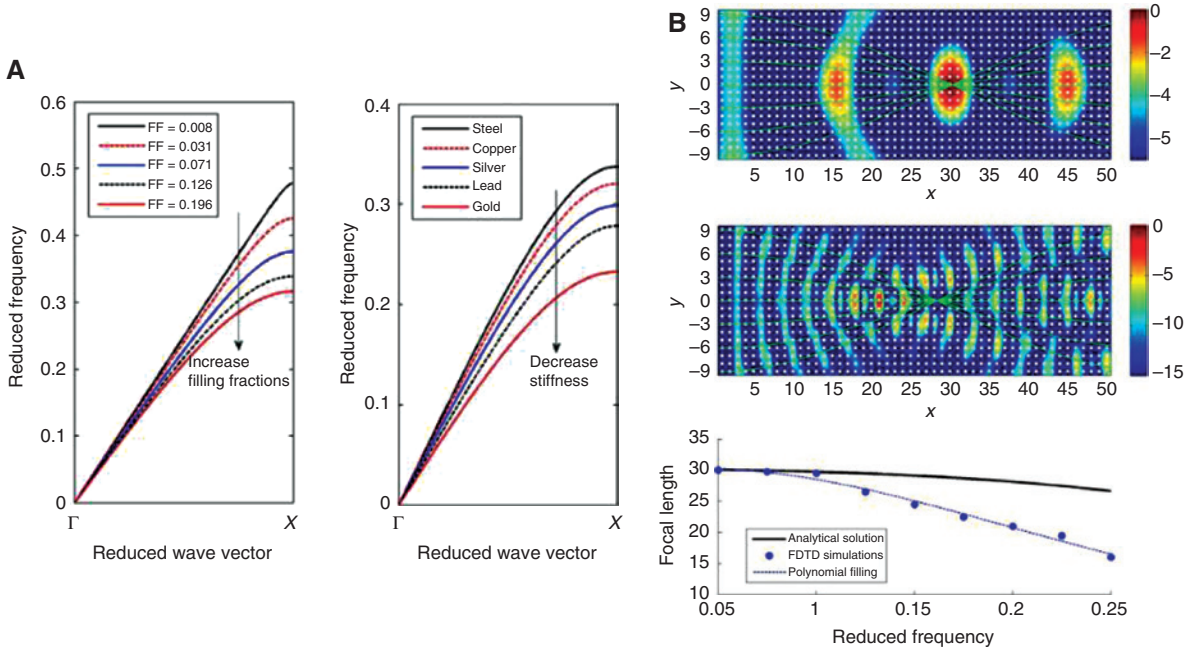

Figure 6: GRIN phononic crystals for bulk elastic waves.
(A) Left: The first shear-vertical (SV) mode of bulk elastic wave along the ΓX for varying the filling fractions of steel cylinders embedded in epoxy. The arrow indicates the increasing of the filling fraction. Right: Same band diagram but for phononic crystals made of different solid material inclusions in epoxy with a fixed filling fraction as 0.126. The arrow indicates the decreasing of stiffness. (B) The finite difference time domain (FDTD) simulated SV wave propagations in a phononic crystal whose inclusions are made of different materials embedded in epoxy at two different frequencies. The calculated and simulated focal lengths as a function of frequency are also plotted as solid line and dotted line, respectively [18].

frequency, and for different bands the dispersive properties of the effective index are slightly different. Therefore, if a GRIN flat lens is designed based on a given frequency, it may have a small deviation in focal length as the effective or fitted gradient coefficient α in Eq. (12) changes, as seen in the right panel of Figure 6.

5 GRIN devices for flexural waves

The control of elastic waves in plates provides the most interesting applications such as on-chip acoustic propagation, thermal conductivity control and opto-mechanic interactions in micro/nanoscale for GRIN devices, which can be attractive for the communities of physics, materials and nano science. For 2D thin plates, or membranes, the elastic waves propagate as surface waves due to the constraints of the plate's two boundaries, resulting in antisymmetric, symmetric and shear-horizontal polarizations. Among those modes, the fundamental antisymmetric mode, in another word flexural mode, is widely studied since it is mainly characterized by out-of-plane displacement component in plates that can be easily detected by means of optical methods.

Figure 7A shows the foci of the GRIN flat lens connected to a linear phononic crystal waveguide for flexural waves in a piezoelectric plate based on deep reactive ion etching. The well-designed GRIN lens focuses a plane incident wave as a spot at the interface between the GRIN lens and the phononic waveguide so that waveguiding is demonstrated. This would have potential for developing active microplate lenses [96]. In Figure 7B, GRIN flat lens is fabricated with silicon pillars erected on top to behave as a metalens to demonstrate the focusing behind the lens in the near-field beyond the diffraction limit. The dipolar resonant pillars and the flexural waves can exhibit polarization coherency to enhance the evanescent waves in order to help the focal spot include better information [68]. The conception of mixed local resonance and GRIN lens can also be applied to other types of waves. At nanoscale, a gradient optomechanical/phoxonic crystal in one-dimensional semiconductor slab is fabricated with the minimum radius of the hole as only 100 nm [78], as displayed in Figure 7C. This phoxonic crystal demonstrates a full phononic band gap at the gigahertz

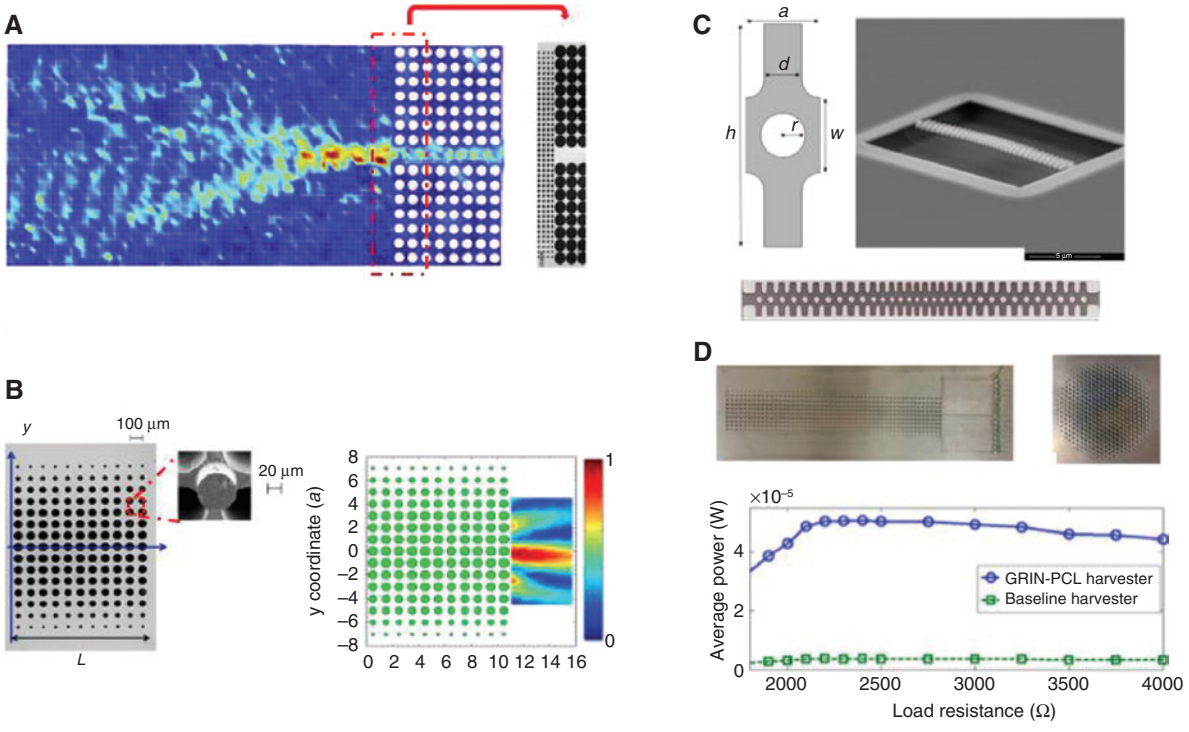

Figure 7: GRIN devices for flexural waves.
(A) Acoustic waveguide by combining GRIN flat lens and phononic crystals in an 80 μm thick plate. SEM image shows samples in the rectangular dotted box with the radii of gradient holes varying from 15 μm to 25 μm [96]. (B) Acoustic metalens by combining GRIN flat lens and pillars (30 μm radius) to exhibit the near-field subdiffraction focusing [68]. (C) 1D phoxonic crystal with varied unit cells (the minimum radius of holes is 100 nm) to exhibit the optomechanical interactions [78]. (D) GRIN flat rectangular lens and Luneburg circular lens for energy harvesting [71, 72].

domain. The optomechanical coupling originates from moving interfaces and the photoelastic effect. The acoustic mode inside the band gap exhibits high mechanical quality factor making the optomechanical phonon coherent manipulation possible. Figure 7D illustrates that the confinement of elastic waves in the GRIN devices can be used for energy harvesting [71, 72]. Piezoelectric energy harvester disks are deposited on a GRIN flat lens and a Luneburg lens at a position where the incident plane wave is focused as a spot. Comparing to the energy harvested in the background plate, the GRIN devices can generate output electrical power an order of magnitude higher.

In Section 3, Eq. (10) gives a useful tool to calculate the effective parameters of phononic crystal plates whose thickness is fixed as a constant. Therefore, GRIN devices can be designed by varying the filling ratio, in other words changing the radii of holes [62]. Now let us revisit the equation of motion (9) which describes flexural waves using Kirchhoff-Love approximation. When a plane wave propagates in a thin plate with a wavenumber k, Eq. (9) gives the solutions for the dispersion relation and phase velocity as

$$k^4 = \frac{\rho h \omega^2}{D},\ c^4 = \left(\frac{\omega}{k}\right)^4 = \omega^2 \frac{Eh^3}{12(1-v^2)\rho h} \tag{14}$$

from where one can see that the phase velocity is not only related to the elastic parameters but also depends on the plate's thickness. This special property of flexural

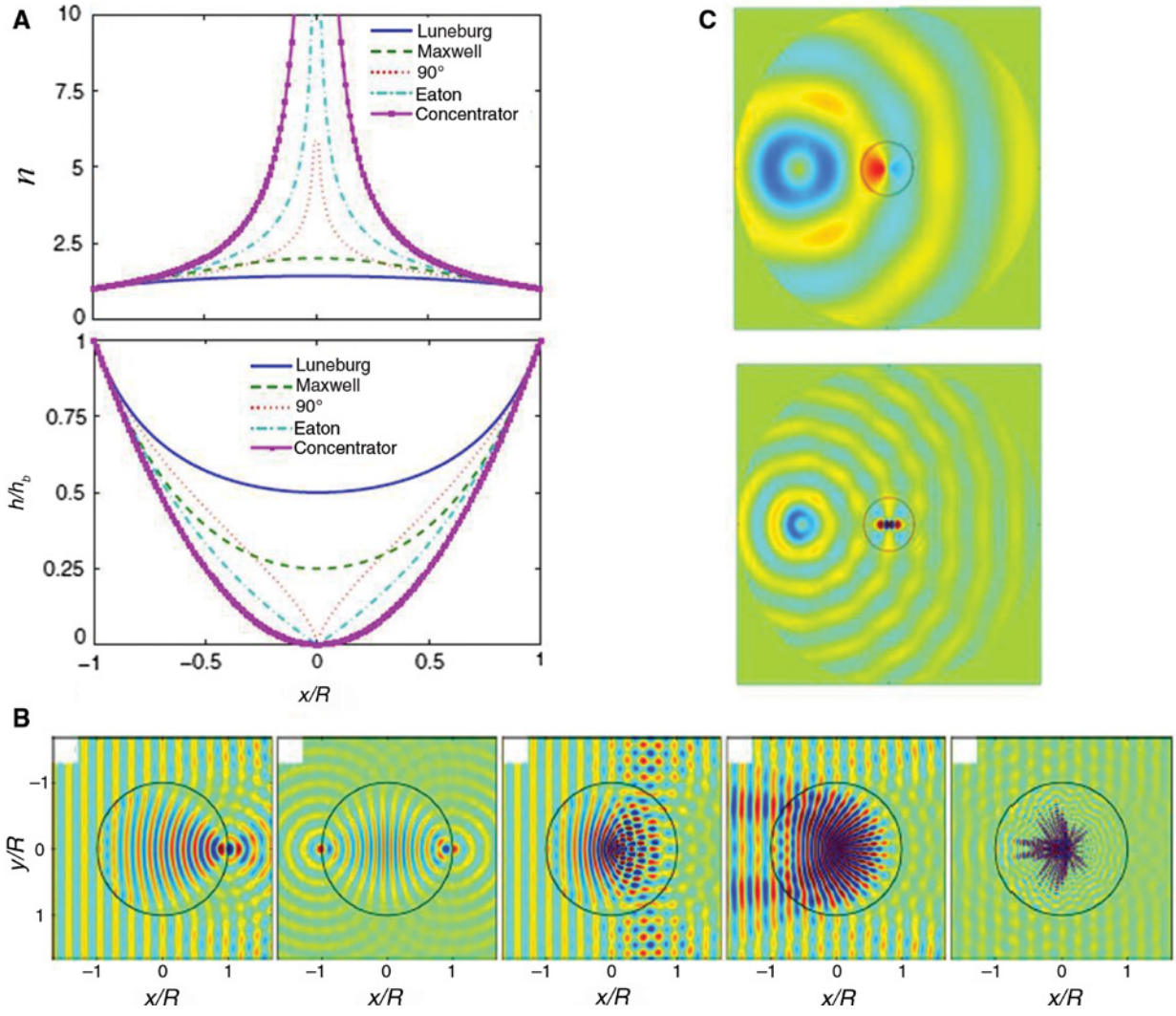

Figure 8: GRIN lenses for flexural waves based on plate's thickness variations.
(A) Refractive index n profiles and corresponding plate's thickness h/h_b variations for Luneburg, Maxwell fish-eye, 90° rotating, Eaton, concentrator lenses. (B) Wave performances of those lenses [24]. (C) Omnidirectional invisible lens for flexural waves based on thickness variation for two different frequencies [64].

waves allows designing of GRIN devices just by locally varying the plate's thickness without any phononic crystal with holes. The refractive index for flexural wave can be easily derived when all elastic parameters remain fixed as in [60]

$$n_{\text{eff}} = \sqrt{\frac{h_b}{h_{\text{eff}}}} \tag{15}$$

In the upper left panel of Figure 8, a set of omnidirectional GRIN devices are displayed with their refractive index profiles, namely, Luneburg, Maxwell fish-eye, 90° rotating, Eaton and concentrator lenses [97, 98], as shown by the different colors. Implementing the refractive formula Eq. (15), their corresponding thickness variations are also shown in the panel below. To achieve higher refractive index n_{eff}, it needs smaller thickness h_{eff}. For 90° rotating, Eaton and concentrator lenses, the maximum index at the center of the circular lens is larger than 5, so that the relative thickness there is smaller than 1/25. The designed GRIN lenses based on thickness variation are performed with full wave simulations, and their corresponding wave functionalities are displayed at the bottom of Figure 8 [24].

Invisibility is always a challenging problem for wave control in physics. Acoustic cloaks in principle require inhomogeneous and anisotropic materials for their realization, which are quite complicated to fabricate in practice [99–101]. A special gradient refractive index profile for omnidirectional invisible lens is derived that requires an infinite index in the vicinity of the center [102, 103]. However, such singularity can be achievable for flexural wave by Eq. (15). Nevertheless, from a practical point of view, the central index can be chosen with a proper finite value in accordance with the step in design. A ray enters the lens and exits in the same direction by flowing a loop around the center inside the lens, thus producing an invisible effect. The multi-frequency performance of the invisible lens is simulated with cylindrical waves from a point source as seen in Figure 8C. [64]. It is worthy to note that acoustic cloak for flexural wave based on nonlinear transformation acoustics method is proposed and realized also by varying the plate's thickness locally to fulfill the required rigidity profile [104].

6 Multimodal GRIN devices

From Figure 3B, the fundamental Lamb modes have another two polarizations in addition to flexural mode. In fact, excitation in the thin plate from a given source will generate all kinds of modes, which means a design for only one mode may hinder the full functionalities of a GRIN device for applications such as absorption and energy harvesting. As discussed in the last section, the flexural wave can be independently controlled by thickness variation for given elastic parameters. The S_0 and SH_0 modes mainly depend on the elastic parameters (c_{11}, c_{13}, c_{33}) and (c_{66}), respectively, for transversely isotropic materials. Therefore, it needs a homogenization theory to obtain the full effective stiffness matrix. As illustrated in Figure 3 in Section 3, the full homogenization method described in Section 2.2 for bulk phononic crystal can be also applied to the thin phononic crystal plate by considering the latter as a finite thin "slice" taken from the former. All the three polarizations of the Lamb waves are well described in the low-frequency limit. Taking the same gold-shell-hole unit cell, we make a sweep for the outer radius while also varying the inner radius for a given outer radius. Figure 9A shows a full phase diagram of all possible pairs of (n_{S0}, n_{SH0}) domain with this sweeping approach, which exhibits several interesting properties: (i) the dotted red line cutting the blue domain indicates that the effective indexes for the S_0 and SH_0 modes are identical, supporting the simultaneous control of these two modes; (ii) the maximum effective index for S_0 mode can reach up to almost 5, while it can be larger than 10 for SH_0 mode; (iii) the wide blue domain shows that it is possible to design a special (n_{S0}, n_{SH0}) trajectory that makes a GRIN device work as one type of lens for S_0 mode and as another lens for SH_0 mode. After defining the index profiles for SH_0 and S_0 modes, the index of A_0 mode can be designed by means of an independent thickness variation and such that it works similarly to the one or both of the SH_0 and S_0 modes or as another totally different lens. Thus, a full control of Lamb modes and advanced multimodal GRIN device becomes achievable.

In Figure 9B, the red dotted circle shows the area of the Maxwell fish-eye lens that is designed to work similarly for all the three fundamental modes. A point source is excited at the left border of the lens, and a focused point image is formed at the right diametric border for a given frequency. It should be mentioned that the wavelengths of the three modes are different since their speeds are not the same due to different dispersion properties. The design of the full control means the positions of point focusing are the same, but not the wave field patterns. Finally, an advanced multimodal GRIN device is displayed in Figure 9C: it works as Luneburg lens for the S_0 and SH_0 modes, while it behaves as Maxwell fish-eye lens for the A_0 mode. The full control method is also extended to GRIN flat lens and beam splitter [63].

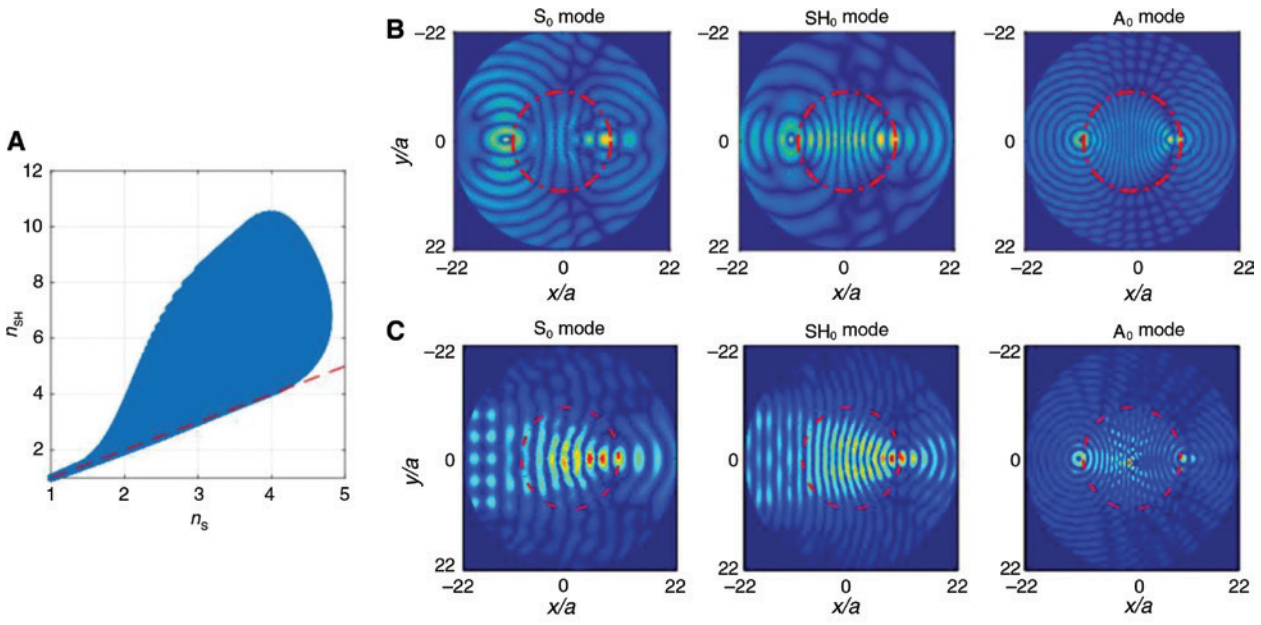

Figure 9: Multimodal GRIN devices to fully control all three fundamental Lamb waves.
(A) Diagram of all possible values for the effective indexes for (n_{S0}, n_{SH0}) by varying the inner and outer radii of the gold-shell-hole structure. (B) GRIN Maxwell fish-eye lens designed for all three Lamb modes simultaneously. (C) An advanced multimodal GRIN device works as Luneburg lens for the S_0 and SH_0 modes while as Maxwell fish-eye lens for the flexural mode [25].

7 Summary

Over the past two decades, we witnessed the rapid growth and development of phononic crystals and metamaterials as well as the recent emergence of metasurfaces to deepen the understanding of wave physics. Although the effective index is a homogenized result from infinite periodic structures, it is still proper to define a local index in a gradient structure, being a bridge between infinity and locality. The homogenization theories of phononic crystals/metamaterials and the design principles of GRIN devices are implemented in terms of wavelength, mainly in long wavelength limit $\lambda > 3\sim4a$, a being the lattice constant. Therefore, the GRIN conception can be applied to the structure's size from nanometer to meter and different wave natures propagating in solids, liquids and gases with free or constrained boundary conditions, among which the applications for elastic waves in thin plates at nanoscales show a promising potential in future for wireless telecommunications, heat conductivity, phonon sensor and so on. The complex properties of elastic waves in thin plates are also fully demonstrated to design more advanced and multimodal GRIN devices. The applications of GRIN phononic crystals and metamaterials are mainly related with energy redirection and focusing; however, more advanced devices could also be considered some subtype of GRIN devices, though their functionality is not designed in the framework of "ray trajectory design". This is the case of acoustic cloaks [100, 105–108], parity-time-symmetric acoustic structures [109–111], one-way acoustic diode [112, 113] and acoustic rainbow trapping [114–116]. Nevertheless, several challenges remain to be answered in future: (1) When wave propagates from one medium to another one, from a uniform surface point of view its behavior is governed by the Snell's law that involves the ratio of the refractive index between the two media. However, the wave energy transfer rate is governed by the impedance ratio between the two media. For some GRIN devices such as flat lens and transmitted-type metasurface, the impedance matching condition is not always easily fulfilled, which will limit the focusing energy level and the corresponding energy harvesting efficiency. (2) New refractive index profiles are needed to discover mathematical methods that can help to design updated wave functionalities. (3) New physics such as thermal conductivity behaviors and nonlinear optical/acoustic responses in gradient phoxonic crystals at nanoscale. It can be foreseen that new breakthroughs will be reported by the united efforts in the communities of physics, material science, engineering, nano science and mathematics among others.

Acknowledgments: Y.J. acknowledges a start-up fund under "Hundred Youth Talent" program from Tongji University. D.T. acknowledges financial support through a "Ramónn y Cajal" fellowship under grant number RYC-2016-21188 and by the "Universitat Jaume I" under project number UJI-A2018-08.

References

[1] Kushwaha MS, Halevi P, Dobrzynski L, Djafari-Rouhani B. Acoustic band structure of periodic elastic composites. Phys Rev Lett 1993;71:2022–5.

[2] Sigalas M, Economou EN. Band structure of elastic waves in two dimensional systems. Solid State Commun 1993;86:141–3.

[3] Liu ZY, Zhang XX, Mao YW, et al. Locally resonant sonic materials. Science 2000;289:1734–6.

[4] Lu M-H, Feng L, Chen Y-F. Phononic crystals and acoustic metamaterials. Mater Today 2009;12:34–42.

[5] Pennec Y, Vasseur JO, Djafari-Rouhani B, Dobrzyński L, Deymier PA. Two-dimensional phononic crystals: examples and applications. Surf Sci Rep 2010;65:229–91.

[6] Hussein MI, Leamy MJ, Ruzzene M. Dynamics of phononic materials and structures: historical origins, recent progress, and future outlook. Appl Mech Rev 2014;66:040802.

[7] Ge H, Yang M, Ma C, et al. Breaking the barriers: advances in acoustic functional materials. Nat Sci Review 2017;5:159–82.

[8] Deymier PA. Acoustic metamaterials and phononic crystals. Berlin, Springer Science & Business Media, 2013.

[9] Khelif A, Adibi A. Phononic crystals: fundamentals and applications. Berlin, Springer, 2015.

[10] Dobrzynski L, Akjouj A, Pennec Y, Al-Wahsh H, Lévêque G, Djafari-Rouhani B. Phononics: interface transmission tutorial book series. Amsterdam, Elsevier, 2017.

[11] Craster RiV, Guenneau S, eds. Acoustic metamaterials negative refraction, imaging, lensing and cloaking. Berlin, Springer Science and Business Media, 2012, pp. 1–318.

[12] Cummer SA, Christensen J, Alù A. Controlling sound with acoustic metamaterials. Nat Rev Mater 2016;1:16001.

[13] Ma G, Sheng P. Acoustic metamaterials: from local resonances to broad horizons. Sci Adv 2016;2:e1501595.

[14] Jin Y, Fernez N, Pennec Y, et al. Tunable waveguide and cavity in a phononic crystal plate by controlling whispering-gallery modes in hollow pillars. Phys Rev B 2016;93:054109.

[15] Jin Y, Torrent D, Djafari-Rouhani B. Robustness of conventional and topologically protected edge states in phononic crystal plates. Phy Rev B 2018;98:054307.

[16] Jin Y, Bonello B, Moiseyenko RP, Pennec Y, Boyko O, Djafari-Rouhani B. Pillar-type acoustic metasurface. Phys Rev B 2017;96:104311.

[17] Torrent D, Sánchez-Dehesa J. Acoustic metamaterials for new two-dimensional sonic devices. New J Phys 2007;9:323.

[18] Lin S-CS, Huang TJ, Sun J-H, Wu T-T. Gradient-index phononic crystals. Phys Rev B 2009;79:094302.

[19] Climente A, Torrent D, Sánchez-Dehesa J. Sound focusing by gradient index sonic lenses. Appl Phys Lett 2010;97:104103.

[20] Martin TP, Naify CJ, Skerritt EA, et al. Transparent gradient-index lens for underwater sound based on phase advance. Phys Rev Appl 2015;4:034003.

[21] Peng S, He Z, Jia H, et al. Acoustic far-field focusing effect for two-dimensional graded negative refractive-index sonic crystals. Appl Phys Lett 2010;96:263502.

[22] Tian Y, Tan Z, Han X, Li W. Phononic crystal lens with an asymmetric scatterer. J Phys D Appl Phys 2019;52:025102.

[23] Yan X, Zhu R, Huang G, Yuan F-G. Focusing guided waves using surface bonded elastic metamaterials. Appl Phys Lett 2013;103:121901.

[24] Climente A, Torrent D, Sánchez-Dehesa J. Gradient index lenses for flexural waves based on thickness variations. Appl Phys Lett 2014;105:064101.

[25] Jin Y, Torrent D, Pennec Y, Pan Y, Djafari-Rouhani B. Gradient index devices for the full control of elastic waves in plates. Sci Rep 2016;6:24437.

[26] Jin Y, Torrent D, Pennec Y, Pan Y, Djafari-Rouhani B. Simultaneous control of the S_0 and A_0 Lamb modes by graded phononic crystal plates. J Appl Phys 2015;117:244904.

[27] Liang Z, Li J. Extreme acoustic metamaterial by coiling up space. Phys Rev Lett 2012;108:114301.

[28] Zhu X, Liang B, Kan W, Peng Y, Cheng J. Deep-subwavelength-scale directional sensing based on highly localized dipolar mie resonances. Phys Rev Appl 2016;5:054015.

[29] Ding Y, Statharas EC, Yao K, Hong M. A broadband acoustic metamaterial with impedance matching layer of gradient index. Appl Phys Lett 2017;110:241903.

[30] Zhu X, Li K, Zhang P, et al. Implementation of dispersion-free slow acoustic wave propagation and phase engineering with helical-structured metamaterials. Nat Commun 2016;7:11731.

[31] Titovich AS, Norris AN, Haberman MR. A high transmission broadband gradient index lens using elastic shell acoustic metamaterial elements. J Acoust Soc Am 2016;139:3357–64.

[32] Yi K, Collet M, Ichchou M, Li L. Flexural waves focusing through shunted piezoelectric patches. Smart Mater Struct 2016;25:075007.

[33] Yong G, Hong-Xiang S, Chen L, et al. Acoustic focusing by an array of heat sources in air. Appl Phys Express 2016;9:066701.

[34] Assouar B, Liang B, Wu Y, Li Y, Cheng J-C, Jing Y. Acoustic metasurfaces. Nat Rev Mater 2018;3:460–72.

[35] Xu Y, Fu Y, Chen H. Planar gradient metamaterials. Nat Rev Mater 2016;1:16067.

[36] Kovalenko A, Fauquignon M, Brunet T, Mondain-Monval O. Tuning the sound speed in macroporous polymers with a hard or soft matrix. Soft Matter 2017;13:4526–32.

[37] Ba A, Kovalenko A, Aristégui C, Mondain-Monval O, Brunet T. Soft porous silicone rubbers with ultra-low sound speeds in acoustic metamaterials. Sci Rep 2017;7:40106.

[38] Jin Y, Kumar R, Poncelet O, Mondain-Monval O, Brunet T. Soft metasurface with gradient acoustic index. In: 11th International Conference of Electrical, Transport, and Optical Properties on Inhomogeneous Media, Krakow, Poland, p. 39, 2018.

[39] Jin Y, Kumar R, Poncelet O, Mondain-Monval O, Brunet T. Flat acoustics with soft gradient-index metasurfaces. Nat Commun 2019;10:143.

[40] Wang Z, Zhang P, Nie X, Zhang Y. Focusing of liquid surface waves by gradient index lens. Europhys Lett 2014;108:24003.

[41] Wang Z, Zhang P, Nie X, Zhang Y. Manipulating water wave propagation via gradient index media. Sci Rep 2015;5:16846.

[42] Climente A, Torrent D, Sánchez-Dehesa J. Omnidirectional broadband acoustic absorber based on metamaterials. Appl Phys Lett 2012;100:144103.

[43] Liang Y-J, Chen L-W, Wang C-C, Chang I-L. An acoustic absorber implemented by graded index phononic crystals. J Appl Phys 2014;115:244513.

[44] Wu L-Y, Chen L-W. An acoustic bending waveguide designed by graded sonic crystals. J Appl Phys 2011;110:114507.

[45] Bao-Guo Y, Ye T, Ying C, Xiao-Jun L. An acoustic Maxwell's fish-eye lens based on gradient-index metamaterials. Chin Phys B 2016;25:104301.

[46] Zhu R, Ma C, Zheng B, et al. Bifunctional acoustic metamaterial lens designed with coordinate transformation. Appl Phys Lett 2017;110:113503.
[47] Zhang Z, Li R-Q, Liang B, Zou X-Y, Cheng J-C. Controlling an acoustic wave with a cylindrically-symmetric gradient-index system. Chin Phys B 2015;24:024301.
[48] Zigoneanu L, Popa B-I, Cummer SA. Design and measurements of a broadband two-dimensional acoustic lens. Phys Rev B 2011;84:024305.
[49] Wu L-Y, Chen L-W. Enhancing transmission efficiency of bending waveguide based on graded sonic crystals using antireflection structures. Appl Phys A 2012;107:743–8.
[50] Li Y, Yu G, Liang B, et al. Three-dimensional ultrathin planar lenses by acoustic metamaterials. Sci Rep 2014;4:6830.
[51] Romero-García V, Cebrecos A, Picó R, Sánchez-Morcillo VJ, Garcia-Raffi LM, Sánchez-Pérez JV. Wave focusing using symmetry matching in axisymmetric acoustic gradient index lenses. Appl Phys Lett 2013;103:264106.
[52] Su X, Norris AN, Cushing CW, Haberman MR, Wilson PS. Broadband focusing of underwater sound using a transparent pentamode lens. J Acoust Soc Am 2017;141:4408–17.
[53] Jahdali RA, Wu Y. High transmission acoustic focusing by impedance-matched acoustic meta-surfaces. Appl Phys Lett 2016;108:031902.
[54] Zhao S-D, Wang Y-S, Zhang C. High-transmission acoustic self-focusing and directional cloaking in a graded perforated metal slab. Sci Rep 2017;7:4368.
[55] Colombi A, Guenneau S, Roux P, Craster RV. Transformation seismology: composite soil lenses for steering surface elastic Rayleigh waves. Sci Rep 2016;6:25320.
[56] Colombi A, Colquitt D, Roux P, Guenneau S, Craster RV. A seismic metamaterial: the resonant metawedge. Sci Rep 2016;6:27717.
[57] Colombi A, Ageeva V, Smith RJ, et al. Enhanced sensing and conversion of ultrasonic Rayleigh waves by elastic metasurfaces. Sci Rep 2017;7:6750.
[58] Jia-Hong S, Yuan-Hai Y. Beam focusing of surface acoustic wave using gradient-index phononic crystals. in: IEEE International Ultrasonics Symposium, Tours France, p. 1–3, 2016.
[59] Zhao J, Bonello B, Becerra L, Boyko O, Marchal R. Focusing of Rayleigh waves with gradient-index phononic crystals. Appl Phys Lett 2016;108:221905.
[60] Climente A, Torrent D, Sánchez-Dehesa J. Omnidirectional broadband insulating device for flexural waves in thin plates. J Appl Phys 2013;114:214903.
[61] Torrent D, Pennec Y, Djafari-Rouhani B. Effective medium theory for elastic metamaterials in thin elastic plates. Phys Rev B 2014;90:104110.
[62] Torrent D, Pennec Y, Djafari-Rouhani B. Omnidirectional refractive devices for flexural waves based on graded phononic crystals. J Appl Phys 2014;116:224902.
[63] Jin Y, Torrent D, Pennec Y, Lévêque G, Pan Y, Djafari-Rouhani B. Multimodal and omnidirectional beam splitters for Lamb modes in elastic plates. AIP Adv 2016;6:121602.
[64] Jin Y, Torrent D, Djafari-Rouhani B. Invisible omnidirectional lens for flexural waves in thin elastic plates. J Phys D Appl Phys 2017;50:225301.
[65] Zhao J, Marchal R, Bonello B, Boyko O. Efficient focalization of antisymmetric Lamb waves in gradient-index phononic crystal plates. Appl Phys Lett 2012;101:261905.
[66] Zareei A, Darabi A, Leamy MJ, Alam M-R. Continuous profile flexural GRIN lens: focusing and harvesting flexural waves. Appl Phys Lett 2018;112:023901.
[67] Zhao J, Bonello B, Boyko O. Beam paths of flexural Lamb waves at high frequency in the first band within phononic crystal-based acoustic lenses. AIP Adv 2014;4:124204.
[68] Zhao J, Bonello B, Boyko O. Focusing of the lowest-order antisymmetric Lamb mode behind a gradient-index acoustic metalens with local resonators. Phys Rev B 2016;93:174306.
[69] Zhao J, Bonello B, Marchal R, Boyko O. Beam path and focusing of flexural Lamb waves within phononic crystal-based acoustic lenses. New J Phys 2014;16:063031.
[70] Wu T-T, Chen Y-T, Sun J-H, Lin S-CS, Huang TJ. Focusing of the lowest antisymmetric Lamb wave in a gradient-index phononic crystal plate. Appl Phys Lett 2011;98:171911.
[71] Tol S, Degertekin FL, Erturk A. Gradient-index phononic crystal lens-based enhancement of elastic wave energy harvesting. Appl Phys Lett 2016;109:063902.
[72] Tol S, Degertekin FL, Erturk A. Phononic crystal Luneburg lens for omnidirectional elastic wave focusing and energy harvesting. Appl Phys Lett 2017;111:013503.
[73] Lin S-CS, Tittmann RB, Sun J-H, Wu T-T, Huang TJ. Acoustic beamwidth compressor using gradient-index phononic crystals. J Phys D Appl Phys 2009;42:185502.
[74] Lin S-CS, Huang TJ. Acoustic mirage in two-dimensional gradient-index phononic crystals. J Appl Phys 2009;106:053529.
[75] Darabi A, Leamy MJ. Analysis and experimental validation of an optimized gradient-index phononic-crystal lens. Phys Rev Appl 2018;10:024045.
[76] Cha J, Daraio C. Electrical tuning of elastic wave propagation in nanomechanical lattices at MHz frequencies. Nat Nanotechnol 2018;13:1016–20.
[77] Hatanaka D, Mahboob I, Onomitsu K, Yamaguchi H. Phonon waveguides for electromechanical circuits. Nat Nanotechnol 2014;9:520.
[78] Gomis-Bresco J, Navarro-Urrios D, Oudich M, et al. A one-dimensional optomechanical crystal with a complete phononic band gap. Nat Commun 2014;5:4452.
[79] Navarro-Urrios D, Capuj NE, Colombano MF, et al. Nonlinear dynamics and chaos in an optomechanical beam. Nat Commun 2017;8:14965.
[80] Wagner MR, Graczykowski B, Reparaz JS, et al. Two-dimensional phononic crystals: disorder matters. Nano Lett 2016;16:5661–8.
[81] Cha J, Kim KW, Daraio C. Experimental realization of on-chip topological nanoelectromechanical metamaterials. Nature 2018;564:229–33.
[82] Milton GW. The theory of composites. Cambridge, UK, Cambridge University Press, 2002.
[83] Torrent D, Håkansson A, Cervera F, Sánchez-Dehesa J. Homogenization of two-dimensional clusters of rigid rods in air. Phys Rev Lett 2006;96:204302.
[84] Torrent D, Sanchez-Dehesa J. Effective parameters of clusters of cylinders embedded in a nonviscous fluid or gas. Phys Rev B 2006;74:224305.
[85] Berryman JG. Long-wavelength propagation in composite elastic media I. Spherical inclusions. J Acoust Soc Am 1980;68:1809–19.
[86] Cervera F, Sanchis L, Sánchez-Pérez JV, et al. Refractive acoustic devices for airborne sound. Phys Rev Lett 2001;88:023902.

[87] Torrent D, Sanchez-Dehesa J. Acoustic metamaterials for new two-dimensional sonic devices. New J Phys 2007;9:323.
[88] Torrent D, Sánchez-Dehesa J, Cervera F. Evidence of two-dimensional magic clusters in the scattering of sound. Phys Rev B 2007;75:241404.
[89] Krokhin AA, Arriaga J, Gumen LN. Speed of sound in periodic elastic composites. Phys Rev Lett 2003;91:264302.
[90] Norris AN, Shuvalov AL, Kutsenko AA. Analytical formulation of three-dimensional dynamic homogenization for periodic elastic systems. Proc Roy Soc A-Math Phy Eng Sci 2012;468:1629–51.
[91] Royer D, Morgan DP, Dieulesaint E. Elastic waves in solids I: free and guided propagation. Berlin Heidelberg, Springer, 1999.
[92] Torrent D, Pennec Y, Djafari-Rouhani B. Resonant and nonlocal properties of phononic metasolids. Phys Rev B 2015;92:174110.
[93] Martin TP, Nicholas M, Orris GJ, Cai L-W, Torrent D, Sánchez-Dehesa J. Sonic gradient index lens for aqueous applications. Appl Phys Lett 2010;97:113503.
[94] Martin TP, Layman CN, Moore KM, Orris GJ. Elastic shells with high-contrast material properties as acoustic metamaterial components. Phys Rev B 2012;85:161103.
[95] Lin S-CS, Tittmann BR, Huang TJ. Design of acoustic beam aperture modifier using gradient-index phononic crystals. J Appl Phys 2012;111:123510.
[96] Chiou M-J, Lin Y-C, Ono T, Esashi M, Yeh S-L, Wu T-T. Focusing and waveguiding of Lamb waves in micro-fabricated piezoelectric phononic plates. Ultrasonics 2014;54:1984–90.
[97] Šarbort M, Tyc T. Spherical media and geodesic lenses in geometrical optics. J Opt 2012;14:075705.
[98] Narimanov EE, Kildishev AV. Optical black hole: broadband omnidirectional light absorber. Appl Phys Lett 2009;95:041106.
[99] Steven AC, David S. One path to acoustic cloaking. New J Phys 2007;9:45.
[100] Torrent D, Sánchez-Dehesa J. Acoustic cloaking in two dimensions: a feasible approach. New J Phys 2008;10:063015.
[101] Chen H, Chan CT. Acoustic cloaking and transformation acoustics. J Phys D Appl Phys 2010;43:113001.
[102] Miñano JC. Perfect imaging in a homogeneous three-dimensional region. Opt Express 2006;14:9627–35.
[103] Tyc T, Chen H, Danner A, Xu Y. Invisible lenses with positive isotropic refractive index. Phys Rev A 2014;90:053829.
[104] Darabi A, Zareei A, Alam MR, Leamy MJ. Experimental demonstration of an ultrabroadband nonlinear cloak for flexural waves. Phys Rev Lett 2018;121:174301.
[105] Cummer SA, Schurig D. One path to acoustic cloaking. New J Phys 2007;9:45–5.
[106] Zhang S, Xia C, Fang N. Broadband acoustic cloak for ultrasound waves. Phys Rev Lett 2011;106:024301.
[107] Zhu X, Liang B, Kan W, Zou X, Cheng J. Acoustic cloaking by a superlens with single-negative materials. Phys Rev Lett 2011;106:014301.
[108] Jin Y, Fang X, Li Y, Torrent D. Engineered diffraction gratings for acoustic cloaking. Phys Rev Appl 2019;11:011004.
[109] Zhu X, Ramezani H, Shi C, Zhu J, Zhang X. $\mathcal{P}\mathcal{T}$-Symmetric acoustics. Phys Rev X 2014;4:031042.
[110] Liu T, Zhu X, Chen F, Liang S, Zhu J. Unidirectional wave vector manipulation in two-dimensional space with an all passive acoustic parity-time-symmetric metamaterials crystal. Phys Rev Lett 2018;120:124502.
[111] Li H-X, Rosendo-Lopez M, Zhu Y-F, et al. Ultrathin acoustic parity-time symmetric metasurface cloak. 2018. arXiv preprint arXiv:1812.05845.
[112] Zhu X, Zou X, Liang B, Cheng J. One-way mode transmission in one-dimensional phononic crystal plates. J Appl Phys 2010;108:124909.
[113] Li R-Q, Liang B, Li Y, Kan W-W, Zou X-Y, Cheng J-C. Broadband asymmetric acoustic transmission in a gradient-index structure. Appl Phys Lett 2012;101:263502.
[114] Zhu J, Chen Y, Zhu X, et al. Acoustic rainbow trapping. Sci Rep 2013;3:1728.
[115] Zhao D-G, Li Y, Zhu X-F. Broadband Lamb wave trapping in cellular metamaterial plates with multiple local resonances. Sci Rep 2015;5:9376.
[116] Peng Y-G, Qin C-Z, Zhao D-G, et al. Experimental demonstration of anomalous Floquet topological insulator for sound. Nat Commun 2016;7:13368.